AIAA JOURNAL
Vol. 38, No. 3, March 2000

Prediction of Rotorcraft Noise with a Low-Dispersion Finite Volume Scheme

Gang Wang* and Lakshmi N. Sankar†
Georgia Institute of Technology, Atlanta, Georgia 30332-0150
and
Hormaz Tadghighi‡
The Boeing Company, Mesa, Arizona 85205-9797

A low-dispersion finite volume (LDFV) scheme on curvilinear meshes is developed and applied to rotorcraft noise prediction. This scheme minimizes the numerical dispersion errors that arise in modeling convection phenomena, while keeping dissipation errors small. It is accomplished by special high-order polynomials that interpolate the properties at the cell centers to the left and right sides of cell faces. A low-pass filter has also been implemented that removes high-frequency oscillations near shock waves. This scheme has been retrofitted into a version of the finite volume code TURNS. The modified solver, referred to as TURNS-LDFV, is shown to yield good results for high-speed impulsive noise applications. The LDFV scheme is also shown to be useful for capturing the blade-tip vortex core structure and its evolution.

Nomenclature

a_k	= stencil coefficients
b, c, d, e	= low-dispersion scheme coefficients
C_Q	= torque coefficient
C_T	= thrust coefficient
E, F, G	= inviscid fluxes
$\boldsymbol{i}, \boldsymbol{j}, \boldsymbol{k}$	= Cartesian unit vectors
$\boldsymbol{n}$	= normal vector of cell surface
q	= vector-valued flow or acoustic variable
q_L, q_R	= left and right upwind variables
R	= radius of rotor blade
R, S, T	= viscous fluxes
r	= stencil increment ratio
S	= surface enclosing a flow cell
t	= time-like variable
V	= flow cell volume
x, y, z	= Cartesian coordinates
α	= wave number
ξ	= computational plane coordinate
Φ	= limiter function

Introduction

HELICOPTERS and tiltrotor vehicles operating near populated areas must have a low noise foot print. To achieve this, the designers must quantify and minimize several aerodynamic noise sources. These sources include loading noise, thickness noise, shock noise, blade-vortex interaction (BVI) noise, and broadband noise. The thickness and loading noise sources can be modeled accurately using Farassat's linearized formulation (known as Formulation 1A).[1] In this approach the rotor-blade thickness and aerodynamic forces are modeled with noncompact monopole and dipole sources, respectively, that rotate and move with reference to an undisturbed medium. However, modeling high-speed impulsive (HSI) noise (also referred to as shock noise) and BVI noise phenomena requires complex nonlinear aerodynamic and acoustic formulations.

The HSI noise is characterized by shocklike structures that emanate from the rotor blade tip and propagate over large distances in the plane of the rotor (Fig. 1). The BVI noise arises from the interaction of the rotor blades with strong vortices shed from a preceding blade (Fig. 2). The rapid variation in induced velocity associated with the interaction between blade and previously shed tip vortex causes large, unsteady variations in pressures near the blade leading-edge region (Fig. 3), resulting in an impulsive noise radiation.

Unlike HSI noise, which is known to propagate mostly in the plane of the rotor, BVI noise propagates out of the rotor disk plane (i.e., typically within the directivity angles of 30–40 deg below the rotor plane). Characteristically, the BVI noise radiation is more audible to an observer on the ground.

Over the past decade much work has addressed the accurate modeling of these noise sources with computational fluid dynamics (CFD) techniques. The near-field details of the flow from the CFD simulations are fed into an aeroacoustic formulation to model the propagation effects to the far field using Kirchhoff's linearized formulation or the Ffowcs Williams and Hawkings (FW-H) equation. For example, Purcell[2] and Srinivasan and Baeder[3] employed the NASA Ames Research Center CFD solver TURNS to investigate HSI noise in hover and forward flight. A spatially third-order accurate form of the Roe scheme with a first-order limiter near shock waves was used in their model. The near-field information from this analysis was subsequently used in a Kirchhoff method[4] to model the pressure field at a far-field observer location. Recently, some researchers have initiated the utilization of the OVERFLOW code in combination with the FW-H equation to model the rotor HSI and BVI noise.[5] During the past decade, researchers have also extensively used full potential flow-based CFD models coupled to a linearized acoustics formulation such as the one in the WOPWOP program.[6] This approach yields fairly accurate predictions of BVI[7] and shock noise phenomena.[8]

However, the classical CFD methods have not found their ways into engineering design because they use very fine body-fitted grids and require significant computational resources to model the flowfield. A fine grid is essential because solutions on coarse grids suffer from two drawbacks: numerical dissipation and dispersion.

Dissipation may be viewed as the progressive decrease in the amplitude of an acoustic wave caused by numerical viscosity as it propagates away from the noise source. This leads to an underprediction of the amplitude of the sound waves. Dispersion may be viewed as the spurious propagation of different frequency components of an acoustic wave at different speeds. It is clear that the

Presented as Paper 99-0480 at the AIAA 37th Aerospace Sciences Meeting, Reno, NV, 11–14 January 1999; received 24 January 1999; revision received 20 July 1999; accepted for publication 22 July 1999.

*Graduate Research Assistant, School of Aerospace Engineering. Student Member AIAA.
†Regents' Professor, School of Aerospace Engineering. Associate Fellow AIAA.
‡Senior Technical Specialist. Senior Member AIAA.

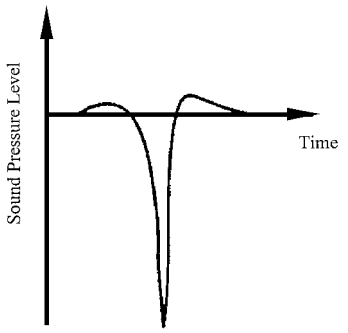

Fig. 1 Wave shape of HSI noise.

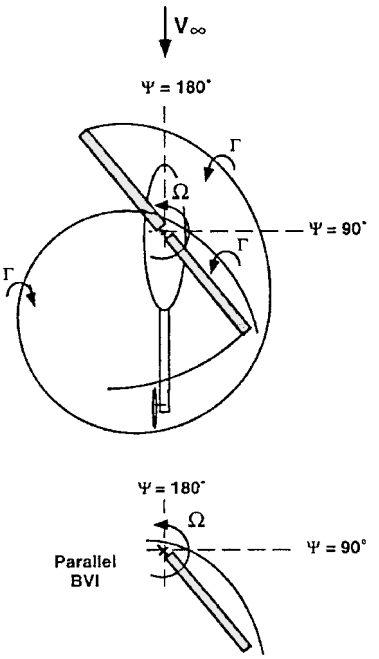

Fig. 2 Schematic of parallel BVI on a helicopter.

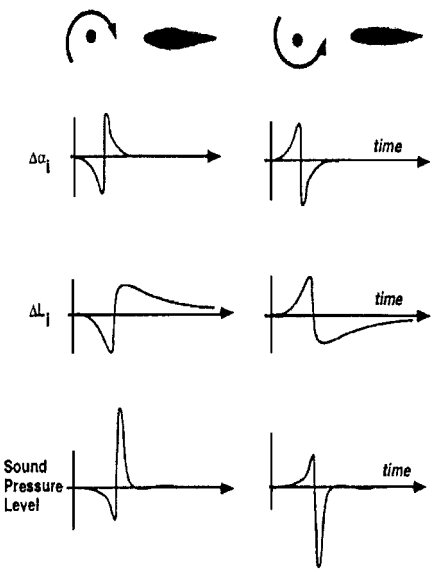

Fig. 3 Source of BVI noise.

traditional numerical schemes are not suitable for the study of wave propagation over long distances and large time intervals. The reduction of the dissipation and dispersion errors hence is essential for an accurate simulation of acoustic wave propagation.

In an attempt to reduce the dispersion errors, Tam[9] and his coworkers developed a low-dispersion numerical scheme called the dispersion-relation-preserving (DRP) finite difference scheme. Although the DRP scheme has superior dispersion characteristics, it has been applied only on Cartesian uniformly spaced grids. Nance[10] and his coworkers developed a low-dispersion finite volume (LDFV) scheme based on the DRP methodology, which may be easily implemented as a variation of the classical third-order Roe type of finite volume scheme on curvilinear grids. This new scheme can be simply realized through the replacement of interpolation expressions for the state vectors at the left q_L and right q_R side of cell faces with new low-dispersion formulas. With this approach good agreement between calculations and exact analytical solutions has been obtained for some classical acoustic problems and for vortex shedding noise emanating from a circular cylinder.[10]

The present work involves the extension and application of the LDFV scheme, hitherto applied only to classical aeroacoustic problems, to the simulation of rotorcraft flow and noise characteristics. To eliminate pre- and postshock oscillations arising near shock waves, an existing limiter (e.g., Roe's Superbee limiter[11]) is applied in conjunction with our high-order LDFV scheme. Results are presented for shock noise and BVI noise applications. Although this algorithm is primarily designed for aeroacoustic problems, this scheme can be effectively used for rotary wing aerodynamics to improve code's ability to accurately capture the blade-tip vortices.

In this paper the aeroacoustic computations are made using TURNS code[3] because it is currently being used as an application tool by both NASA and the industry for rotor aerodynamic design improvements. The existing third-order MUSCL scheme in TURNS was replaced with the present LDFV scheme. The full description of the LDFV implementation in TURNS code is presented here. Enhanced computed aeroacoustic results obtained for a generic model rotor are correlated against measured data.

Mathematical and Numerical Formulation

Navier–Stokes Solver

The TURNS code has been modified to model the acoustic noise phenomenon. The conservation form of three-dimensional Navier–Stokes governing equation may be written as

$$\frac{\partial q}{\partial t}+\frac{\partial E}{\partial x}+\frac{\partial F}{\partial y}+\frac{\partial G}{\partial z}=\frac{\partial R}{\partial x}+\frac{\partial S}{\partial y}+\frac{\partial T}{\partial z} \tag{1}$$

This equation is solved in the divergence form:

$$\frac{\partial}{\partial t}\iiint q\,\mathrm{d}V+\oiint (E\boldsymbol{i}+F\boldsymbol{j}+G\boldsymbol{k})\cdot\boldsymbol{n}\,\mathrm{d}S = \oiint (R\boldsymbol{i}+S\boldsymbol{j}+T\boldsymbol{k})\cdot\boldsymbol{n}\,\mathrm{d}S \tag{2}$$

The inviscid fluxes crossing the cell face are evaluated in this finite volume formulation using Roe's upwind-biased, flux-difference scheme. In the original TURNS code the van Leer MUSCL[12] approach (Fig. 4) is used to obtain higher-order accuracy:

$$q_L = q_i + \tfrac{1}{3}(q_{i+1}-q_i) + \tfrac{1}{6}(q_i - q_{i-1})$$
$$q_R = q_{i+1} - \tfrac{1}{6}(q_{i+2}-q_{i+1}) - \tfrac{1}{3}(q_{i+1}-q_i) \tag{3}$$

A flux limiter is applied on the right-hand side of the equation to remove unexpected high-frequency numerical oscillations near shock waves. The MUSCL scheme is third-order accurate in space.

Low-Dispersion Scheme

In the current research work the LDFV scheme replaces the MUSCL Scheme. We refer to the modified code as TURNS-LDFV and the original TURNS code as TURNS-MUSCL. The goal of the

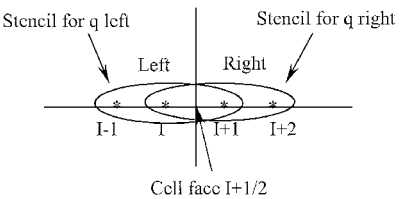

Fig. 4 Stencil for three-point scheme.

LDFV scheme (which is an extension of the concepts in Tam's original DRP scheme) is to choose a proper interpolation that accurately represents, at the cell faces where fluxes are computed, sinusoidal waves of short wavelengths. Details about the LDFV scheme can be found in Ref. 10. Let us try to approximate $q^L_{i+1/2}$ in the transformed uniform plane with five points:

$$q^L_{i+\frac{1}{2}} \approx \tilde{q}^L_{i+\frac{1}{2}} = a_{-2}q_{i-2} + a_{-1}q_{i-1} + a_0 q_i + a_1 q_{i+1} + a_2 q_{i+2} \tag{4}$$

Using classical Taylor series method, we can obtain five expansion equations of $q_{i-2}, q_{i-1}, q_i, q_{i+1}$, and q_{i+2} about $\xi_{i+1/2}$, for example,

$$q_{i+1} = q_{i+\frac{1}{2}} + \sum_{m=1}^{\infty} \frac{q^{(m)}_{i+\frac{1}{2}}}{m!}\left(\frac{1}{2}\Delta\xi\right)^m \tag{5}$$

Compared to the traditional method to construct a higher-order scheme, we only employ four of these five equations to determine coefficients a_k. Another restriction required by the low-dispersion scheme is to match the Fourier transform of approximation for $q^L_{i+1/2}$ with its exact transform. Taking the Fourier transform of Eq. (4), we get the dispersion relation

$$1 \cong \sum_{k=-2}^{2} a_k \exp\left(i\left(k - \frac{1}{2}\right)\alpha\Delta\xi\right) \tag{6}$$

Here α is the wave number. The quantity Q defined next is, therefore, a measure of the errors in the approximation

$$Q = 1 - \sum_{k=-2}^{2} a_k \exp\left(i\left(k - \frac{1}{2}\right)\alpha\Delta\xi\right) \tag{7}$$

The goal of the present LDFV scheme is to minimize Q for all possible values of $\alpha\Delta\xi$ in the range between $-\pi/2$ and $+\pi/2$. This is achieved by minimizing the integral

$$E = \int_{-\pi/2}^{\pi/2} \left\| \sum_{k=-2}^{2} a_k \exp\left(i\left(k - \frac{1}{2}\right)\alpha\Delta\xi\right) - 1 \right\|^2 \mathrm{d}(\alpha\Delta\xi) \tag{8}$$

with respect to the coefficients a_k,

$$\frac{\partial E}{\partial a_k} = 0, \qquad k = -2, \ldots, 2 \tag{9}$$

The notation $\|\cdot\|$ indicates the modulus of a complex number.

The interpolation coefficients a_k are obtained by combining one minimization equation from Eq. (9) with four equations from classical Taylor-series expansions of the right-hand side of Eq. (4) about $\xi_{i+1/2}$. This makes the scheme fourth-order accurate in space. One can exactly solve for interpolation coefficients a_k using a symbolic mathematics program such as Maple reference. The left and right interpolation formulas used in our current research are

$$\begin{aligned} q_L = q^L_{i+\frac{1}{2}} &= q_i + b_L\Phi^+_{i-\frac{3}{2}}(q_{i-1} - q_{i-2}) + c_L\Phi^+_{i-\frac{1}{2}}(q_i - q_{i-1}) \\ &\quad + d_L\Phi^-_{i+\frac{1}{2}}(q_{i+1} - q_i) + e_L\Phi^-_{i+\frac{3}{2}}(q_{i+2} - q_{i+1}) \\ q_R = q^R_{i+\frac{1}{2}} &= q_{i+1} - b_R\Phi^+_{i-\frac{1}{2}}(q_i - q_{i-1}) - c_R\Phi^+_{i+\frac{1}{2}}(q_{i+1} - q_i) \\ &\quad - d_R\Phi^-_{i+\frac{3}{2}}(q_{i+2} - q_{i+1}) - e_R\Phi^-_{i+\frac{5}{2}}(q_{i+3} - q_{i+2}) \end{aligned} \tag{10}$$

where coefficients b_L, c_L, d_L, and e_L are obtained from the corresponding coefficients in Eq. (4). Coefficients b_R, c_R, d_R, and e_R can be determined with the same method. The symbol Φ represents a limiter function needed to remove unwanted nonphysical oscillations in the vicinity of sharp gradients (e.g., shocks). The Superbee limiter proposed by Roe[11] was used:

$$\Phi^+_{i-\frac{1}{2}} = \Phi\left(r^+_{i-\frac{1}{2}}\right), \qquad \Phi^-_{i+\frac{1}{2}} = \Phi\left(r^-_{i+\frac{1}{2}}\right) \tag{11}$$

where

$$r^+_{i-\frac{1}{2}} = \frac{q_{i+1} - q_i}{q_i - q_{i-1}}, \qquad r^-_{i+\frac{1}{2}} = \frac{q_i - q_{i-1}}{q_{i+1} - q_i} \tag{12}$$

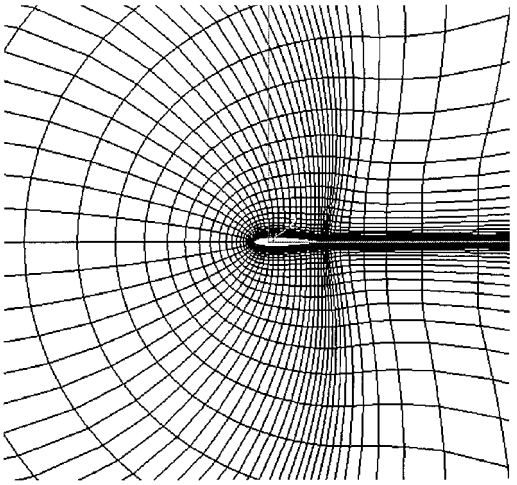

Fig. 5 Schematic of grid in the cylindrical plane perpendicular to the rotor blade.

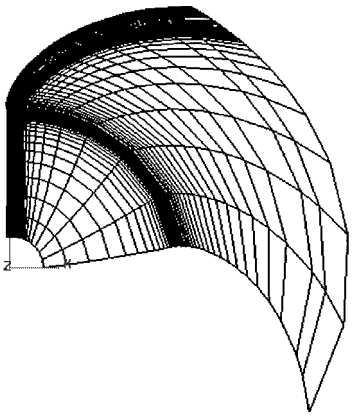

Fig. 6 Schematic of grid in the plane of the rotor blade.

$$\Phi(r) = \max[0, \min(2r, 1), \min(r, 2)] \tag{13}$$

Computational Grid

A hyperbolic C-H grid generator supplied with the TURNS code is used in all of the calculations. The three-dimensional grid is constructed from a series of two-dimensional C grids with an H-type topology in the spanwise direction. The grid is clustered in the vicinity of the rotor-blade surface, with a sparse distribution of the points away from the blade (Fig. 5). For accurate modeling of the shock delocalization phenomena, the grid generator automatically clusters the nodes near the expected location of the shock surface (Fig. 6), as predicted by linear theories.

Results and Discussion

In this section the LDFV scheme just described is applied to shock noise and BVI noise problems. Results from the original code (TURNS-MUSCL) and the modified flow solver (TURNS-LDFV) are presented. All TURNS-MUSCL and TURNS-LDFV calculations are done on identical grids to eliminate grid density differences from clouding the comparisons. Results are also presented for a lifting rotor in hover to demonstrate the tip vortex capturing capabilities of the LDFV scheme.

Shock Noise Prediction

Calculations have been performed for a two-bladed UH-1H rotor in hover. The blades are untwisted and have a rectangular plan form with NACA 0012 airfoil sections and aspect ratio of 13.71. The sound pressure levels have been compared to the experimental data for a $\frac{1}{7}$ scale model, as discussed by Purcell.[2]

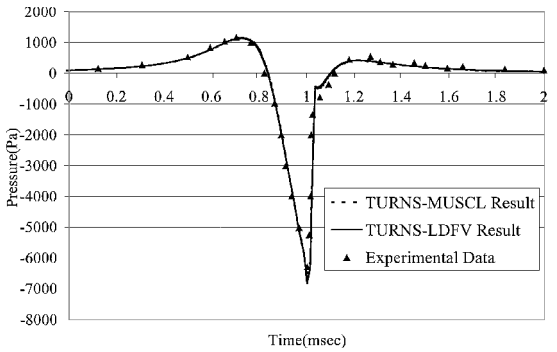

Fig. 7 Shock noise prediction: $M_{tip} = 0.90$, $r/R = 1.111$, and grid size 133 × 45 × 31.

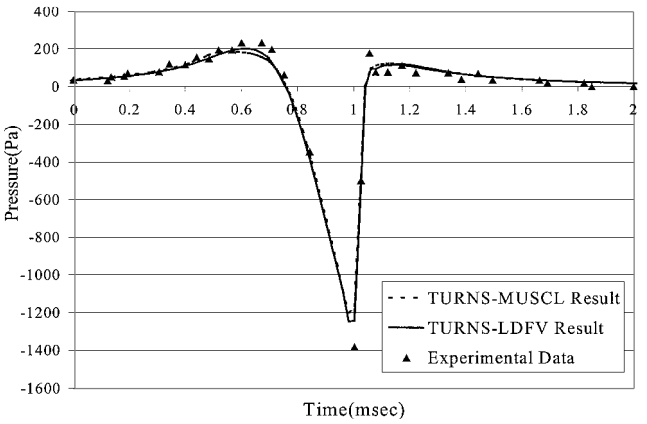

Fig. 8 Shock noise prediction: $M_{tip} = 0.90$, $r/R = 1.78$, and grid size 133 × 45 × 31.

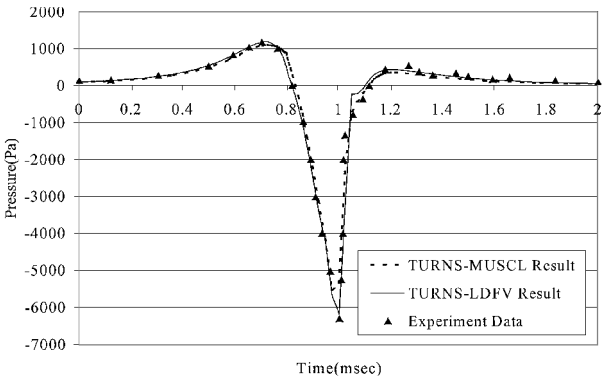

Fig. 9 Shock noise prediction: $M_{tip} = 0.90$, $r/R = 1.111$, and grid size 75 × 45 × 31.

Case 1: Tip Mach Number $M_{tip} = 0.90$

As a first step in validating the LDFV scheme, the TURNS-LDFV and TURNS-MUSCL calculations were done on a 133 × 45 × 31 computational grid, similar to the grid used in Ref. 13. The pressure field at two stationary microphone locations $r = 1.11R$ and $1.78R$ were extracted from the flow simulations as a function of time. The calculations are compared with the measured data (Figs. 7 and 8). As depicted, on this relatively fine grid TURNS-LDFV and TURNS-MUSCL both yield nearly the same results, and the predictions compare very well with the experimental data. The negative acoustic pressure peak, a salient feature of HSI noise signal, as well as the asymmetry of the pressure signal are predicted fairly accurately.

To determine how the TURNS-MUSCL and the TURNS-LDFV methodologies behave on a coarser grid, the calculations for flow conditions shown on Figs. 7 and 8 were repeated on a 75 × 45 × 31 grid. This grid was constructed by removing every other point in the streamwise direction over the rotor-blade span from the original 133 × 45 × 31 grid. Figures 9 and 10 show the results using the coarse grid. From the computed results it is clear that the TURNS-LDFV predictions correlate better with the experimental data compared to TURNS-MUSCL in the near field ($r/R = 1.11$). However, at larger distances from rotor hub (e.g., $r/R = 1.78$) the highly stretched and coarse grid induces a significant dissipation in the computed flow, and both schemes cannot accurately capture the magnitude of negative pressure peak. In relative terms the negative acoustic peak pressure is underestimated by 20% using TURNS-LDFV and by 28.6% with the TURNS-MUSCL scheme. It demonstrates that TURNS-LDFV still behaves better that TURNS-MUSCL.

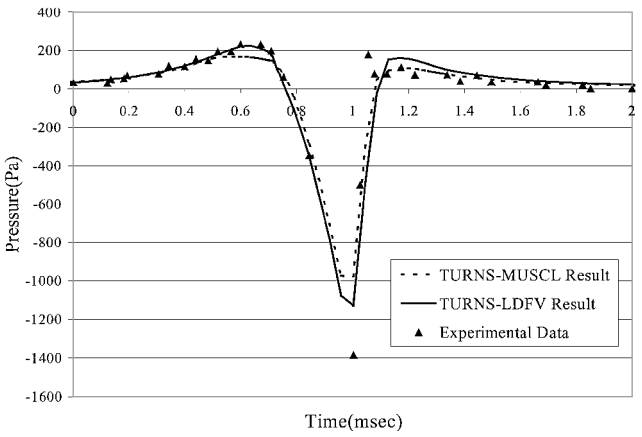

Fig. 10 Shock noise prediction: $M_{tip} = 0.90$, $r/R = 1.78$, and grid size 75 × 45 × 31.

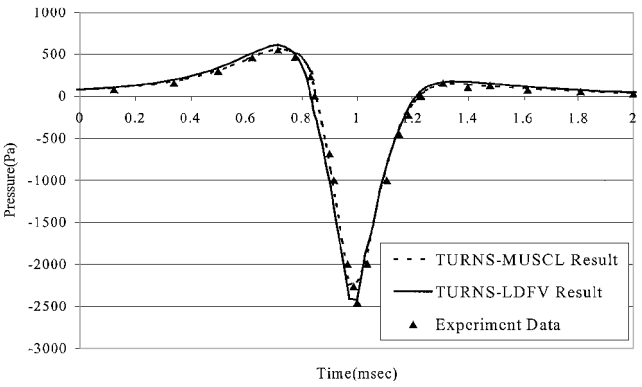

Fig. 11 Shock noise prediction: $M_{tip} = 0.88$, $r/R = 1.136$, and grid size 75 × 45 × 31.

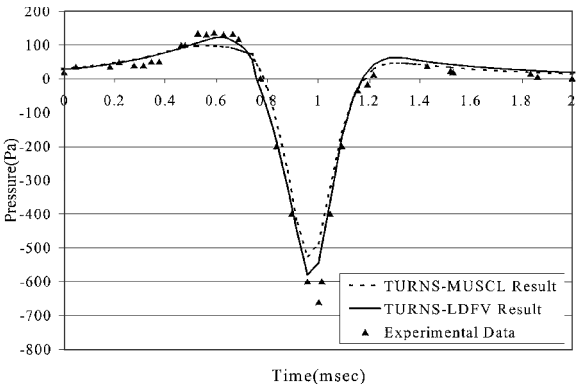

Fig. 12 Shock noise prediction: $M_{tip} = 0.88$, $r/R = 1.78$, and grid size 75 × 45 × 31.

Case 2: Tip Mach Number $M_{tip} = 0.88$

At lower tip Mach numbers, using coarse grid, the agreement between the TURNS-LDFV calculations and the experiment is considered good, as shown in Figs. 11 and 12. At this tip Mach number the shock wave appears to start to become delocalized. Both the

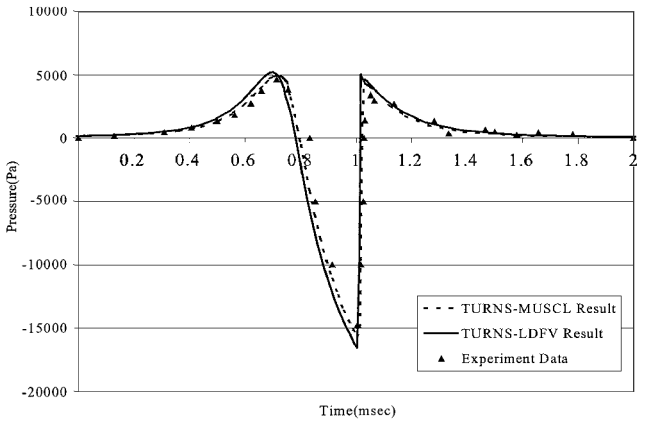

Fig. 13 Shock noise prediction: $M_{tip} = 0.95$, $r/R = 1.0526$, and grid size 75 × 45 × 31.

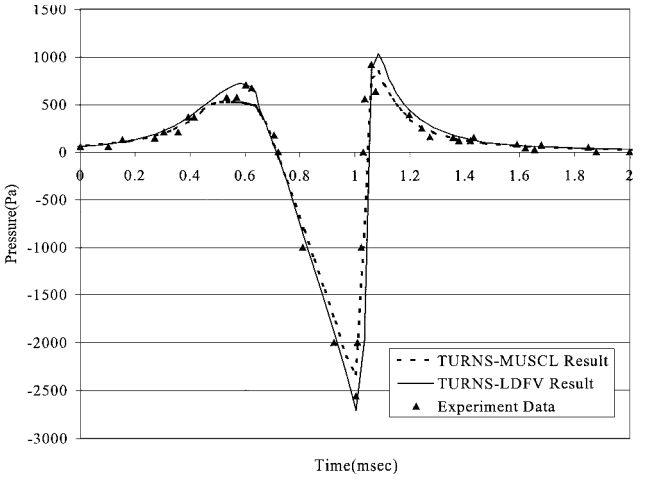

Fig. 14 Shock noise prediction: $M_{tip} = 0.95$, $r/R = 1.78$, and grid size 75 × 45 × 31.

experimental data and numerical simulation wave depict a more symmetrical form of the acoustic pressure p' vs time, in contrast to the results for the higher tip Mach number (i.e., $M_{Tip} = 0.9$). The higher the tip Mach number, the more asymmetrical will be the acoustic pressure distribution with respect to time, i.e., the more the shock wave is delocalized. It is encouraging that on coarse grids the negative pressure peak at $r/R = 1.78$ is underpredicted by only 13.4% using TURNS-LDFV in comparison with the TURNS-MUSCL computation, which underestimates the peak by 22.4%.

Case 3: Tip Mach Number M_{tip} = 0.95

At higher tip Mach numbers, using a coarse grid, the agreement between the TURNS-LDFV calculations and the experiment is also better than that of TURNS-MUSCL result, as shown in Figs. 13 and 14.

BVI Noise Prediction

The Kitaplioglu-Caradonna[14] parallel BVI experiment (Fig. 15) is next modeled with the TURNS-LDFV solver. The two-bladed, teetering rotor has a diameter of 7.125 ft. The blade is untwisted, has a rectangular planform, and utilizes 6-in. chord NACA 0012 airfoil sections. The hover tip Mach number is 0.70, and the advance ratio is 0.2. The computational grid consists of 169 points in the wraparound direction with 121 points on the blade surface, 45 points in the radial direction with 23 radial locations on the blade surface, and 57 points in the normal direction, to closely match the TURNS-MUSCL simulations presented in Ref. 15. In the numerical simulations presented here, the line vortex is located 0.25 chord above the blade.

The computed acoustic pressure time history at the microphone 7 location (Fig. 16) with the TURNS-LDFV and TURNS-MUSCL schemes is shown in Fig. 17. The experimental data are also shown. The TURNS-MUSCL results and the experimental data were extracted by digitizing the figures given in Ref. 15. Both the TURNS-LDFV and TURNS-MUSCL schemes have captured the main characteristics of BVI noise signature (i.e., the impulsive nature of the blade airloads caused by the BVI). In this case the vortex first induces an upwash and then a downwash velocity on the blade. This gives rise to a steep positive pressure peak first, followed by a negative pressure peak. Further, the blade thickness geometry induces a noticeable increase in the BVI negative peak value, in agreement with the results given in Ref. 15. TURNS-LDFV computation of the negative pressure peak magnitude is considered good compared with the measured data. However, the positive peak value is somewhat overestimated. One plausible explanation for the overestimation of the positive peak is the way that the trajectory of the upstream-generated vortex was modeled in the TURNS-LDFV code. The vortex has been assumed as a straight-line vortex that remains unaffected in velocity profile and undisturbed in location when it encounters the blade. This is in contrast to the experimental observation that the vortex tends to follow streamlines of the flowfield and is slightly distorted by the interaction with the blade. In addition, the rotor itself is affected by the vortex-sheet wake shed from the upstream vortex generator.

The predicted BVI pulse width, considered as the time elapsed (or the change in the blade azimuthal position ψ) between the positive and negative peaks, is greater than the measured data. There is also a shift in the phase between the computed and the experimental data, for both the TURNS-MUSCL calculations from Ref. 15 and the present TURNS-LDFV calculations. Reference 15 provides an explanation of possible causes for this discrepancy.

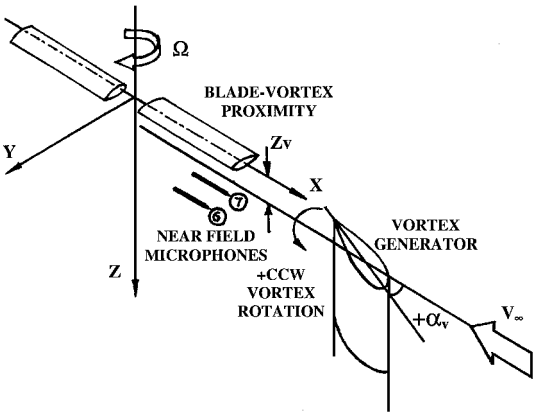

Fig. 15 Schematic of experimental setup in wind-tunnel test section.

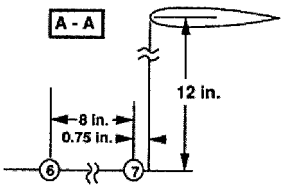

Fig. 16 Position of microphone 7.

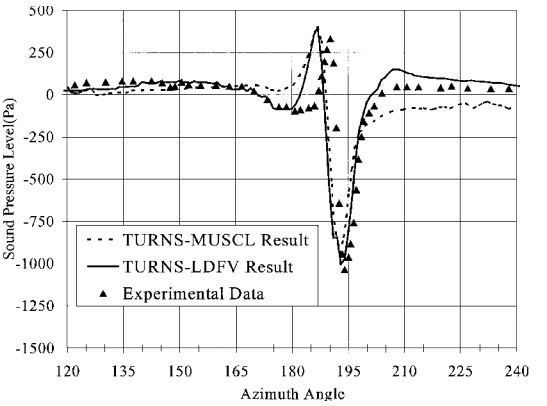

Fig. 17 BVI noise prediction (microphone 7) $M_{tip} = 0.70$, and grid size 169 × 45 × 57.

The TURNS-MUSCL results taken from the Ref. 15 indicate that the MUSCL scheme considered in the BVI analysis lacks needed accuracy to capture the BVI peak-to-peak amplitude. The pressure levels also do not recover the original undisturbed state quickly after the BVI. The TURNS-LDFV scheme, on the other hand, appears to predict the salient features of the BVI pulse with better accuracy using an identical grid employed for the TURNS-MUSCL analysis. The pressure recovery after the negative pressure peak is slightly overpredicted with TURNS-LDFV, but it is overall in better correlation with the experimental data than the TURNS-MUSCL prediction.

Tip Vortex Structure Prediction Capabilities of TURNS-LDFV

Although the TURNS-LDFV scheme has been developed with aeroacoustic applications in mind, it also offers an enhanced capability for aerodynamic applications, given its high formal spatial accuracy and low-dissipation/dispersion characteristics. In support of the preceding statement, aerodynamic results for a rotor in hover are presented. The case selected for this study is the classical hovering rotor experimental data documented by Caradonna and Tung.[16] Calculations were performed at a rotor collective pitch angle of 8 deg and a tip Mach number of 0.44. The computational grid is coarse and consisted of 79 points in the wraparound direction with 21 points on the blade surface, 45 points in the radial direction with 21 radial locations on the blade surface, and 31 points in the normal direction.

Figure 18 (Ref. 17) shows the typical wake pattern for a hovering rotor. There are an inboard vortex sheet and a strong helical vortex shed from the preceding blade tip. The trailing vortices descend down at a slower rate compared to the inboard vortex sheet. There is also some contraction of the rotor wake with the increase in vortex age.

Vorticity magnitude contours in a cutting plane 90 deg behind the blade, as predicted by TURNS-MUSCL and TURNS-LDFV, are shown in Fig. 19. Two distinct vortices can been detected in the rotor wake domain. The smallest one with highest vorticity magnitude is shed from the blade 90 deg ahead of the cutting plane. The second vortex that is just below the rotor-blade plane is shed from the preceding blade now at 270-deg azimuth. This vortex, which has the 270-deg vortex age, is greatly dissipated in the TURNS-MUSCL computational simulation. However, it is clearly captured by the TURNS-LDFV scheme. From this figure the conclusion can be made that the TURNS-LDFV scheme can resolve the tip vortices better than the TURNS-MUSCL scheme even on a coarse grid.

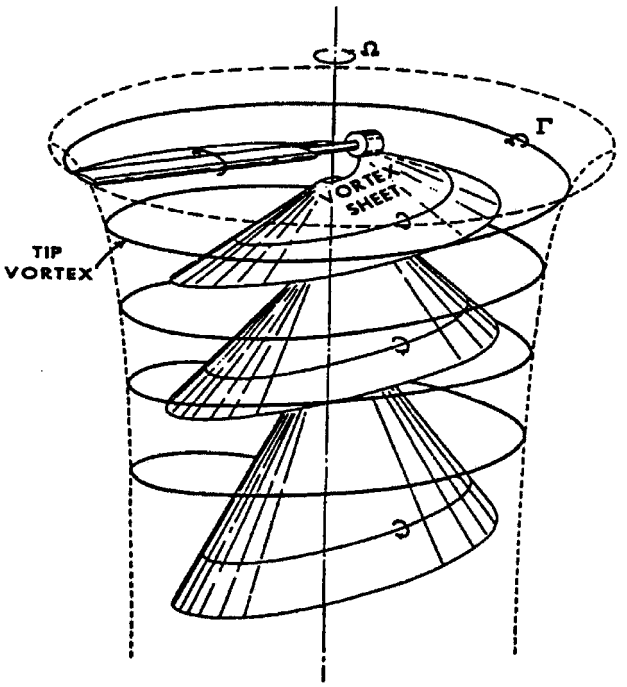

Fig. 18 Schematic of hover rotor wake structure.

Table 1 Computed and measured loads for the Caradonna–Tung rotor on a coarse grid

r/R	TURNS	TURNS-LDFV	Experiment data
0.50	0.2028	0.2120	0.2345
0.68	0.2418	0.2799	0.2815
0.80	0.2609	0.2844	0.2886
0.89	0.2669	0.2834	0.3143
0.96	0.2457	0.2600	0.2683

Table 2 Comparisons of thrust and torque coefficient on a coarse grid

Coefficient	TURNS	TURNS-LDFV	Experiment data
C_T	0.004143	0.004449	0.00459
C_Q	0.001153	0.001177	(not available)

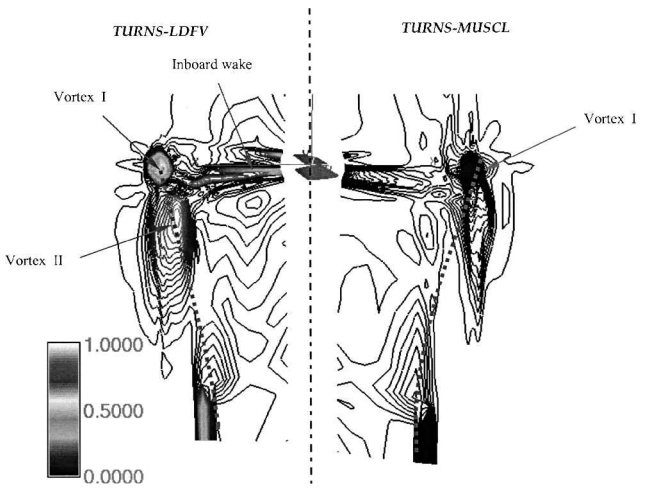

Fig. 19 Vorticity magnitude contour predicted by TURNS-LDFV and TURNS-MUSCL.

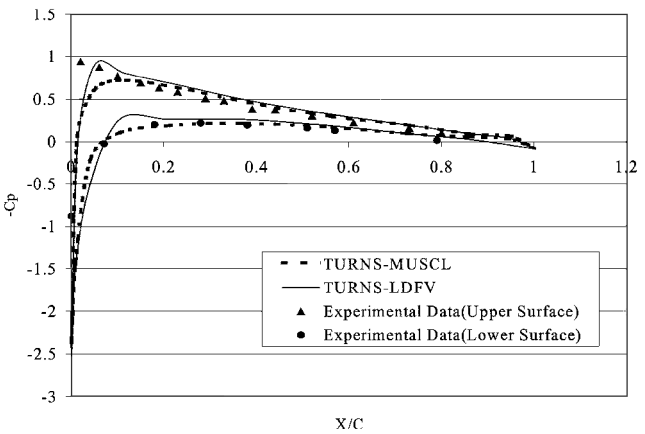

Fig. 20 Comparison of surface pressure coefficient distribution: $M_{tip} = 0.44$ and $r/R = 0.68$.

In addition to the tip vortex computational enhancements, Fig. 19 shows that the inboard vortex sheet is also resolved in a more accurate fashion using TURNS-LDFV scheme up to a vortex age of 180 deg on a coarse grid.

The surface pressure distributions at several radial locations are shown in Figs. 20–22. On the coarse grid that has been employed, the TURNS-LDFV scheme behaves better near the leading-edge suction region of the blade than the TURNS-MUSCL scheme. As a consequence, the sectional lift coefficients and the thrust coefficient obtained by TURNS-LDFV are closer to experimental data. Tables 1 and 2 compare the TURNS-MUSCL and TURNS-LDFV predictions for the sectional lift coefficients and the rotor thrust with experimental data.

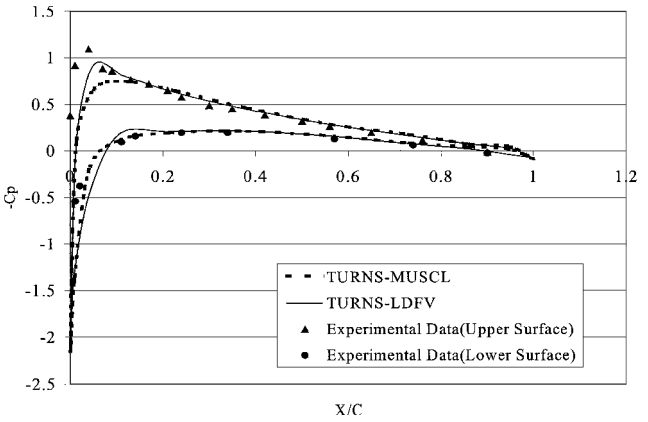

Fig. 21 Comparison of surface pressure coefficient distribution: $M_{tip} = 0.44$ and $r/R = 0.80$.

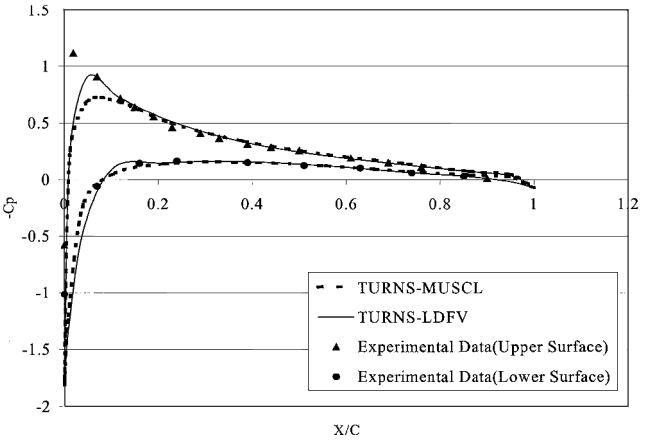

Fig. 22 Comparison of surface pressure coefficient distribution: $M_{tip} = 0.44$ and $r/R = 0.96$.

Srinivasan et al.[3] have done a similar calculation using the TURNS-MUSCL scheme with one million computational grid points and obtained excellent correlation with the measured data. However, such fine grid calculations are not always feasible in engineering applications because of their prohibitive cost. The TURNS-LDFV scheme, on the other hand, appears to yield acceptable results on engineering-quality coarse grid.

Conclusion

A LDFV scheme has been implemented in the TURNS code to accurately predict rotorcraft noise. This scheme is fourth-order accurate in space and first-order accurate in time. A limiter is incorporated in the scheme to remove unwanted nonphysical oscillations from the numerical solutions of nonlinear problems. Encouraging agreement between the predicted results and experiment data has been obtained for shock noise prediction on a coarse grid. The basic characteristics of BVI noise are also captured with satisfactory accuracy. Although intended for aeroacoustic applications, the TURNS-LDFV scheme does a good job of modeling aerodynamic phenomena. Compared to the original TURNS-MUSCL scheme, the TURNS-LDFV scheme can significantly improve the resolution of the tip vortex magnitude and core size on coarse grid.

Additional investigations of BVI noise and tip vortex structure predictions are now in progress with the TURNS-LDFV scheme. This scheme can be easily ported to other industry-standard methods and algorithms such as OVERFLOW or CFL3D in a straightforward manner.

Acknowledgments

This work was supported by the National Rotorcraft Technology Center. Yung Yu was the technical monitor.

References

[1]Farassat, F., "Theory of Noise Generation from Moving Bodies with an Application to Helicopter Rotors," NASA TR R-451, Dec. 1975.

[2]Purcell, T. W., "A Prediction of High-Speed Rotor Noise," AIAA Paper 89-1130, April 1989.

[3]Srinivasan, G. R., Baeder, J. D., Obayashi, S., and McCroskey, W. J., "Flow-Field of a Lifting Rotor in Hover: A Navier–Stokes Simulation," *AIAA Journal*, Vol. 30, No. 10, 1992, pp. 2371–2378.

[4]Farassat, F., and Myers, M. K., "Extension of Kirchhoff's Formula to Radiation from Moving Surfaces," *Journal of Sound and Vibration*, Vol. 123, No. 3, 1988, pp. 451–461.

[5]Strawn, R. C., Ahmad, J., and Duque, E. P. N., "Rotorcraft Aeroacoustics Computations with Overset Grid CFD Methods," *Journal of the American Helicopter Society*, Vol. 44, No. 2, 1999, pp. 132–140.

[6]Brentner, K. S., "Prediction of Helicopter Rotor Discrete Frequency Noise," NASA TM-87721, Oct. 1986.

[7]Visintainer, J. A., Burley, C. L., Marcolini, M. A., and Liu, R. L., "Acoustic Predictions Using Pressures from a Model Rotor in the DNW," *Journal of the American Helicopter Society*, Vol. 38, No. 3, 1993, pp. 35–44.

[8]Brentner, K. S., and Holland, P. C., "An Efficient and Robust Method for Computing Quadrupole Noise," *Journal of the American Helicopter Society*, Vol. 42, No. 2, 1997, pp. 172–181.

[9]Tam, C. K. W., and Webb, J. C., "Dispersion-Relation-Preserving Schemes for Computational Aeroacoustics," *Journal of Computational Physics*, Vol. 107, No. 2, 1993, pp. 262–281.

[10]Nance, D. V., Viswanathan, K., and Sankar, L. N., "Low-Dispersion Finite Volume Scheme for Aeroacoustic Applications," *AIAA Journal*, Vol. 35, No. 2, 1997, pp. 255–262.

[11]Roe, P. L., "Some Contributions to the Modeling of Discontinuous Flows," *Large-Scale Computations in Fluid Mechanics*, edited by B. E. Engquist, S. Osher, and R. C. J. Somerville, Vol. 22, Pt. 2, Lectures in Applied Mathematics, American Mathematical Society, Providence, RI, 1985, pp. 163–193.

[12]Van Leer, B., "Towards the Ultimate Conservative Difference Scheme, V: A Second Order Sequel to Godunov's Method," *Journal of Computational Physics*, Vol. 32, No. 1, 1979, pp. 101–136.

[13]Baeder, J. D., Gallman, J. M., and Yu, Y. H., "A Computational Study of the Aeroacoustics of Rotors in Hover," *Journal of the American Helicopter Society*, Vol. 42, No. 1, 1997, pp. 39–53.

[14]Kitaplioglu, C., Caradonna, F. X., and Burley, C. L., "Parallel Blade-Vortex Interactions: An Experimental Study and Comparison with Computations," *Journal of the American Helicopter Society*, Vol. 42, No. 3, 1997, pp. 272–281.

[15]McCluer, M. S., "Helicopter Blade-Vortex Interaction Noise with Comparisons to CFD Calculations," NASA TM 110423, Dec. 1996.

[16]Caradonna, F. X., and Tung, C., "Experimental and Analytical Studies of a Model Helicopter Rotor in Hover," NASA TM 81232, Sept. 1981.

[17]Gray, R. B., "An Aerodynamic Analysis of a Single-Bladed Rotor in Hovering and Low Speed Forward Flight as Determined from Smoke Studies of the Vorticity Distribution in the Wake," Dept. of Mechanical and Aerospace Engineering, Aeronautical Engineering Rept. 356, Princeton Univ., Princeton, NJ, Sept. 1956, p. 65.

P. J. Morris
Associate Editor